Equivalent Electrical Modeling Approach of a Free Piston Stirling Engine

Gwyddyon Féniès[a], Fabien Formosa[a], Julien Ramousse[b] and Adrien Badel[a]

[a] Univ. Savoie Mont Blanc, SYMME, F-74000 Annecy, France, Gwyddyon.Fenies@univ-savoie.fr
[b] Univ. Savoie Mont Blanc, LOCIE, F-73376 Le Bourget du Lac, France

Abstract:

A model of a three-phase free pistons Stirling engine coupled to its heat sources is proposed in this study. It combines two sub-models: a thermal one for the sources coupling and a dynamic one for the determination of the operating performances such as the frequency, the oscillation amplitude, the compression and expansion power. The dynamic model is based on electrical analogies for each component of the engine. The gas pressure and flow rate are thus represented by voltage and current respectively.
This model has been validated thanks to a comparison with experimental data. An experimental test bench has been built to record measurements and to evaluate the performances of a three-phase free pistons Stirling engine previously developed in our lab. The agreement between the theoretical and experimental performances is demonstrated, with a mean error of 9 %.
The mechanical to electrical power conversion is also taken into account in the model. An electrical model is built to be easily integrated in the dynamic model and to predict the electrical power. Studying the influence of three main parameters (the dead volume of the chambers, the resonance frequency of the mechanical oscillator and the thermal insulation between the cold and the hot sides) a first optimization is performed. It has been determined that a useful power of 20 W could be achieved, for an internal pressure of 2 bar, a chamber volume of 50 cm^3, an oscillating mass of 1.6 kg and a conduction resistance of 8.96 K/W.

Keywords:

Stirling engine, double acting, free piston, equivalent electrical model, waste heat recovery.

1. Introduction

More and more works are dedicated to the waste heat recovery from industrial process, especially aiming at low grade heat associated to low or medium temperature under 200 °C. A way to harvest this energy is to use thermodynamic cycles [1] whose performance are intrinsically limited by the Carnot efficiency (typically 38 % for T_c = 20 °C and T_h = 200 °C).
Commercially available Stirling engines are dedicated to cogeneration applications, with an output power ranging from 1 to 9 kW, at relatively high temperature (650-800 °C) [1]. Whereas Stirling cycle is theoretically very promising, the complexity of this technology lies in the mandatory high performance heat exchangers, regenerator and the endurance of the engine mechanical linkages. However, reasonable performances are now reached compared to Organic Rankin Cycle (ORC) and Thermoelectric (TE) systems [1]. These considerations justify the need for a reliable simple and efficient design for Stirling engine dedicated to low temperature applications. A review of low temperature difference (LTD) Stirling engines was proposed in [2] and [3]. They can reach the requirements of high reliability with low cost realization. Double acting architecture is especially suitable to aim at the highest power density. A free piston double-acting arrangement which does not need complex mechanical linkage was originally suggested by Walker [4]. A way to further increase the reliability of this system is to use membranes instead of pistons. By doing this, all friction losses are avoided whilst ensuring an efficient sealing. Fig. 1 shows the specific architecture of a three-phase double acting free piston engine [4] using membranes.
In his work, Der Minassians proposed a simple LTD double acting free piston engine using membranes [5,6]. Its operation has been demonstrated on a 3 x 31.9 cm^3 displacement prototype.

Air was used at atmospheric pressure and a maximum efficiency of 19.7 % (70 % of the Carnot efficiency) was theoretically anticipated.

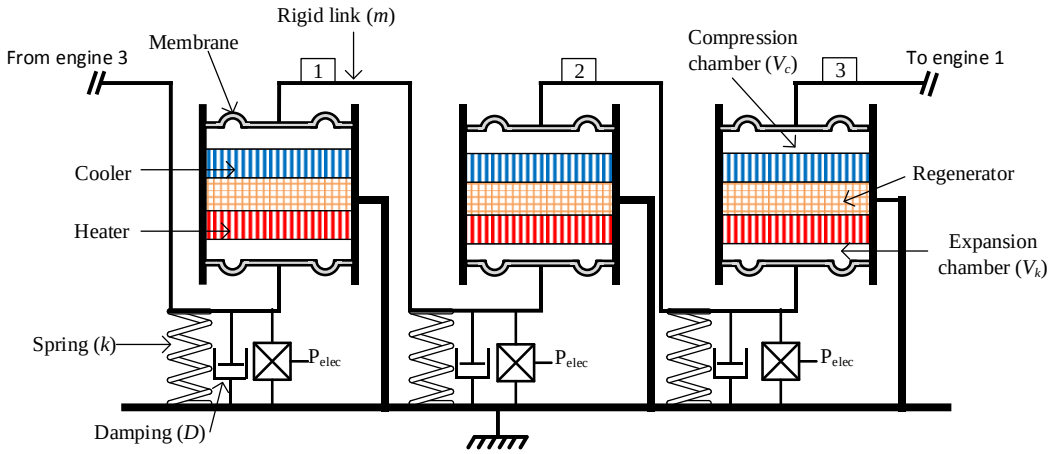

Fig. 1. Schematic of a free piston multi-cylinder double acting Stirling engine

The apparent simplicity of these double acting free piston engine is misleading. Indeed, the operation amplitude and operating frequency are related to a strong coupling between the thermodynamics and mechanical dynamics. Various models for Stirling Engine are available in the literature. The elementary Schmidt analysis theory [2] is based on the assumptions of isothermal compression and expansion and perfect regeneration. Another model was proposed by Urieli [7] assuming adiabatic transformations in the chambers and isothermal heat exchangers. These standard models do not take into account the mechanical dynamics and are then inadequate for the analysis of free piston engines. Der Minassians in [5,6] has developed a model starting from the Schmidt analysis and taking into account the engine's dynamical equilibrium. We proposed an equivalent electrical network model (EENM) in [8] for preliminary design and performances assessment. It lies in the analogy between the thermodynamics' variables (pressure, volumetric flow rate) and the electrical variables (voltage, current). This analogy, derived from the thermo-acoustic theory [9], allows the gas mass and momentum equilibriums to be formulated using basic electrical components (capacitors, resistors and inductances) easily interfaced with the mechanical-electrical analogy. It is then possible to represent the whole engine and derive the linearized transfer function of the system to establish the operating conditions.
In the present work, the EENM is improved: the gas inertia as well as the non-linear effect within the heat exchangers and the regenerator are taken into account; an electromagnetic transducer is added for electromechanical conversion. Moreover, the isothermal assumption underlying the model means that the chamber's temperatures are fixed though the heat transfer coefficients were not taken into account in [8]. The proposed EENM is then interfaced with a thermal model to account for the cycle mean temperatures evaluation of the chambers for given fixed external temperatures. The validation of the model is performed using experimental data carry out by an instrumented Stirling engine prototype. In a second part, the model is used to evaluate performances for optimization purposes.

2. Model description

2.1. Equivalent Electrical Network Model (EENM)

The modeling strategy is based on a division of one phase in its multiple parts namely the expansion chamber, the heater, the regenerator, the cooler and the compression chamber (Fig. 1) considered as 1D spaces. A perfect gas assumption is used whereas isothermal evolutions are considered in the

chambers. Then, for small harmonic variations of the variables (pressure and gas flow rate), the linearized mass and momentum conservation equations are established. Equivalent electrical components (capacitor, resistor and inductor) are then identified. The derived EENM of one phase of the engine is presented in Fig. 2.
The engine's parts geometry, the mean pressure (p_m), the internal temperatures (T_e, T_k for expansion and compression chamber respectively) allow the evaluation of the components.

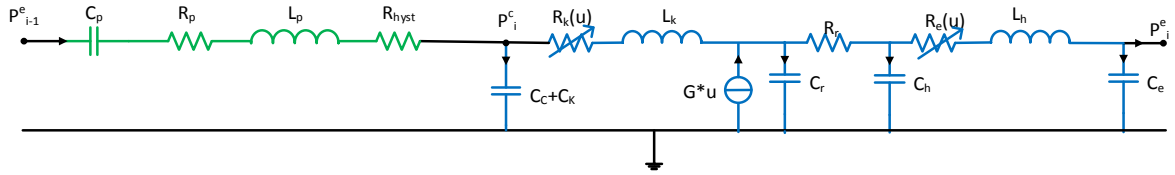

Fig. 2. Equivalent Electrical Model of one phase

In a previous work [8] the authors introduced such a model applied to a double acting multiphase Stirling engine. Some substantial evolutions are introduced here: i) the gas inertia is introduced. Indeed, comparing the thermal penetration length ($\delta = \sqrt{k_g/(\rho_g c_p \omega)}$) to the hydraulic radius of the heat exchangers, the inertia of the gas appears to be significant and is integrated to the model as inductors L_k and L_h in Fig. 2, ii) in the previous model, the components values have been considered constant. In the present work, the evolution of the pressure drops with respect to the gas flow rate amplitude is taken into account using variable resistors (R_k and R_e in Fig. 2), iii) the expression of the losses in the exchangers has also been improved.
From the thermoacoustic theory [10] the pressure drops can be estimated. However, the complex geometry of the heat exchangers in the double acting engine (holed punched plates fitted together as can be seen in Fig. 6c) calls for a more effective experimental identification procedure. Nam in [11] shows that pressure drops in grids are not linear but depend on the square of the volume flow rate. Then, the chosen expression of the pressure drops in the exchangers is expressed as:

$$\Delta p_e(t) = (a + b|u_e(t)|)u_e(t). \qquad (1)$$

In which $u_e(t)$ is the instantaneous gas velocity. The linear a coefficient in (1) is obtained from theoretical approach, $a = \frac{\mu\, l_e}{d\, A_e \sqrt{\frac{2\mu}{\omega\rho}}}$. b will be used as an identification parameter for the model validation. Then, the equivalent electrical resistance standing for the losses in the exchanger defined as $\frac{\Delta P_e}{u_e}$, is:

$$R_e\big(u_e(t)\big) = a + b|u_e(t)| \qquad (2)$$

Finally, the dynamic equilibrium equation is set for the moving parts enclosing one expansion and one compression chambers. A constant capacitor C_p and inductor L_p account for the stiffness and the inertia respectively whereas R_p represents the mechanical losses.

2.2. Electromagnetic transducer

The mechanical energy is converted into electrical energy with an electromagnetic generator. The generator can be obviously represented as an electrical circuit. The transducer coupled equations from [12] are :

$$\frac{(m+m_t)}{{A_p}^2}\dot{v} + \frac{(D+D_t)}{{A_p}^2}v + \frac{(k+k_t)}{{A_p}^2}\int v + \frac{\beta}{A_p} i = p^e_{j-1} - p^c_j \qquad (3)$$

$$R_c i = \frac{\beta}{A_p} v - L_{em}\frac{di}{dt} - r_{em} i \qquad (4)$$

Where v is the volume flow rate and i the current in the electrical circuit, β is the electromechanical coupling ratio. The latest depends on the magnetic flux and the geometry of the generator.

A transformer can represent the electromagnetic transduction, but in this circuit the current has the role of the voltage and the voltage the current. By doing this, the analogy between the current and the volume flow rate is respected. The modified electrical circuit is given in Fig. 3.

This transformation allows the mechanical to electrical energy conversion to be easily added to the main electrical network developed previously (Fig. 2).

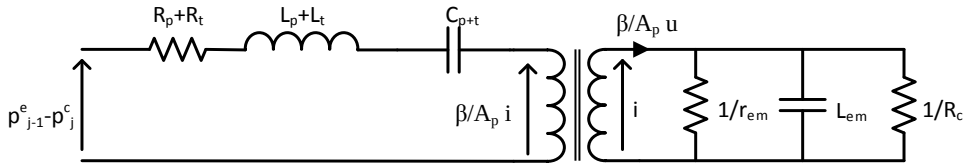

Fig. 3. Equivalent circuit for the electromechanical conversion

The voice coil architecture appears to be well suited for the engine. In [13], such an electromagnetic transducer has been characterized to be joined in a thermoacoustic engine. Its characteristics are used in the model.

2.3. Thermal modelling

The EENM is based here on the continuity equation and momentum equilibrium only. The assumed constant temperatures of the chambers must then be related to the heat transfer from and to the sources. The following strategy details the inclusion of the thermal heat transfers in the model.

The simple Newton law is used to account for the exchange between the gas in the chamber and the cold and hot parts of the engine. It is assumed that, in the range of volume flow rate, the convective coefficient is not depending on the flow rate. The evolution of the heat transfer coefficients with the flow rate could however be included provided that the correlation between the two is established.

From a thermal point of view, a single phase of the double acting engine can be seen as the combination of four elements, as shown in Fig. 4. The "inside" temperatures (T_e, T_k) values used in the EENM are partly driven by the heat transfers at the hot and cold side with the heat sources at T_h and T_c respectively. They are modeled by the thermal resistance R_{thh} and R_{thc} (Fig. 3). The other crucial effect taken into account is the thermal leakage from the hot to the cold side. It is described thanks to the additional thermal resistance R_{cond} (Fig. 4).

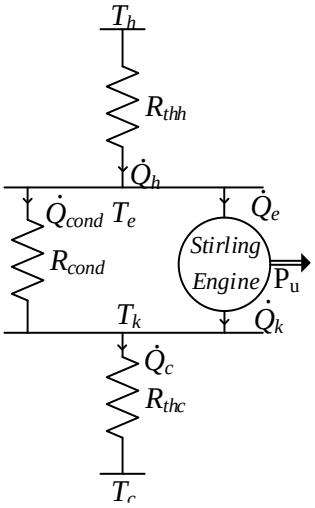

Fig. 4. Thermal Model of one single phase of the double acting engine

From the scheme of Fig. 4, the energy conservation is given by the following expressions:

$$\dot{Q}_h = \frac{(T_h - T_e)}{R_{thh}} = \dot{Q}_e + \dot{Q}_{cond} = \dot{Q}_e + \frac{(T_e - T_k)}{R_{cond}} \qquad (5)$$

$$\dot{Q}_c = \frac{(T_k - T_c)}{R_{thc}} = \dot{Q}_k + \dot{Q}_{cond} = \dot{Q}_k + \frac{(T_e - T_k)}{R_{cond}} \qquad (6)$$

Where the heat flux $\dot{Q}_h$, $\dot{Q}_c$, $\dot{Q}_{cond}$ are given in Fig. 4.

A first estimation of T_e and T_k can be obtained considering a stalled engine ($\dot{Q}_e = \dot{Q}_k = 0$). By doing this, the "stalled" heat flux $\dot{Q}_s$ can be expressed as:

$$\dot{Q}_s = \frac{1}{R_{thh} + R_{cond} + R_{thc}} (T_h - T_c) \qquad (7)$$

The "inside stalled" temperatures T_{es} and T_{ks} are then:

$$T_{es} = T_h - \frac{R_{thh}(T_h - T_c)}{R_{thh} + R_{cond} + R_{thc}} \qquad (8)$$

$$T_{ks} = T_c + \frac{R_{thc}(T_h - T_c)}{R_{thh} + R_{cond} + R_{thc}} \qquad (9)$$

These values will be used to initialize the undetermined internal temperatures T_e and T_k for the resolution as detailed in the next section.

2.4. Resolution strategy

The EENM of the engine is implemented in the Matlab® Simscape environment as shown in Fig. 5.

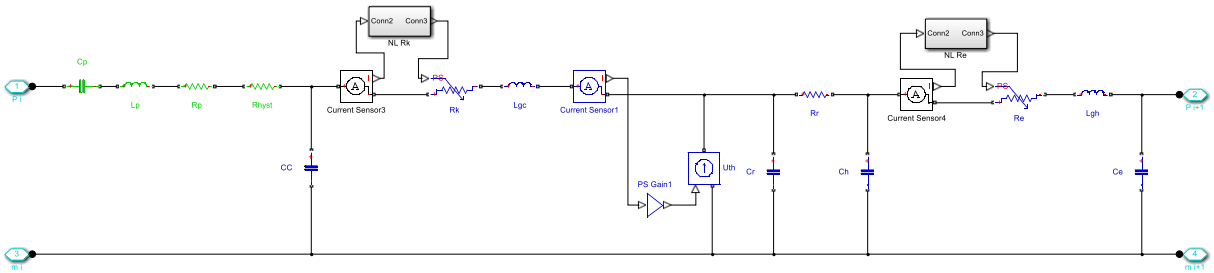

Fig. 5. EENM coded on MATLAB® for one phase

From the "stalled" temperatures values derived from the thermal model, EENM simulation is performed and time-dependent evolutions of the variables (pressure, flow rate) are evaluated. The input power of the expansion chamber $\dot{Q}_e$, and the output power of the compression chamber $\dot{Q}_k$ can be calculated eventually. The chambers' temperatures T_e and T_k are then evaluated again after the current iteration i = 1 using eq. (5-6) (subscript *ni*). If the relative deviation between the current and the previous values is greater than a given precision (typically 10^{-7}), one more iteration i+1 is done again with the input values given by eq. (10-11):

$$T_{e\,i+1} = \frac{T_{ei} + 9T_{eni}}{10} \qquad (10)$$

$$T_{k\,i+1} = \frac{T_{ki} + 9T_{kni}}{10} \qquad (11)$$

It takes about 17 iterations to converge. In order to ease the simulation procedure, a polynomial law is preferred for the equivalent resistance in the exchangers:

$$R_e\big(u_e(t)\big) = a + b'(u_e(t))^2 \qquad (12)$$

The parameter *b'* is supposed to be constant in the range of studied volume flow rate.

3. Model validation

3.1. Prototype description

The prototype presented in [8] was modified. Sensors have been implemented in order to record temperatures, pressures and accelerations, as shown in Fig 6. The hot and cold sides are thermally regulated. The engine has not demonstrated the electromechanical conversion yet as its main purposes is the model validation for performance prediction.

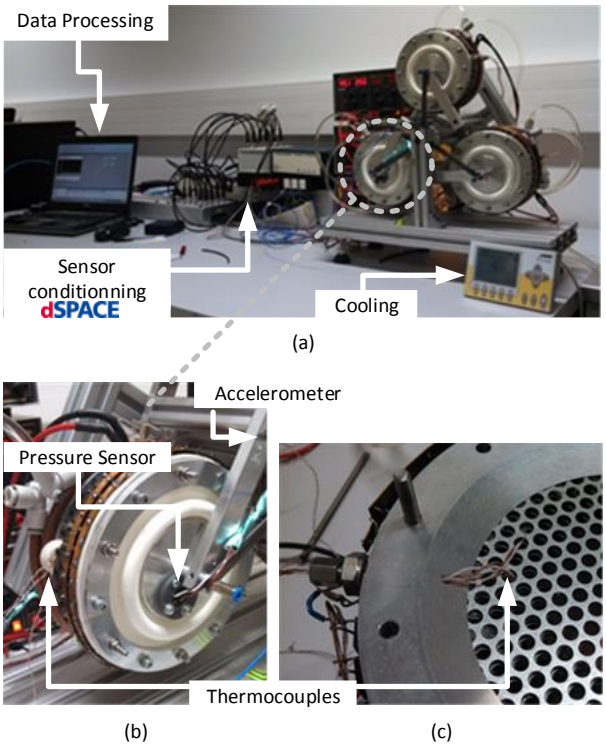

Fig. 6. (a) Global view of the experimental setup and (b, c) close up of the engine instrumentation

3.2. Model parameters identification

Five parameters have to be identified: the damping ratio of the mechanical part (D), the nonlinear pressure drops coefficients (b_e', b_k') and the heat exchange coefficients (h_c, h_h).

D has been experimentally determined through a ring-down test on the mechanical parts isolated from the whole engine. Consequently, the damping ratio has been calculated at D = 5.5 Ns/m ±6 %.

The remaining parameter's values determination is based on a comparison between experimental data and computational model. The comparison variables are: the operating variables (displacement amplitude *amp*, operating frequency *f*), the expansion chamber temperature T_e and post treatment powers $\dot{Q}_e$ and $\dot{Q}_k$. They are integrated in a cost function expressed as:

$$e = \frac{\left|\dot{Q}_{c_{max}}^{exp} - \dot{Q}_{c_{max}}^{th}\right|}{\dot{Q}_{c_{max}}^{exp}} + \frac{\left|\dot{Q}_{e_{max}}^{exp} - \dot{Q}_{e_{max}}^{th}\right|}{\dot{Q}_{e_{max}}^{exp}} + \frac{\left|amp^{exp} - amp^{th}\right|}{amp^{exp}} + \frac{\left|f^{exp} - f^{th}\right|}{f^{exp}} + \frac{\left|{T_e}^{exp} - {T_e}^{th}\right|}{{T_e}^{exp}} + \frac{\left|{T_k}^{exp} - {T_k}^{th}\right|}{{T_k}^{exp}} \qquad (13)$$

The minimization of e is sought optimizing the values of b_e', b_k', h_h and h_c. The minimum is reached for: $b_e' = 2.9.10^{10}$ Pa.s.m^{-3}, $b_k' = 2.4.10^{10}$ Pa.s.m^{-3}, $h_h = 10\pm5$ W/(m^{2}K) and $h_c = 100\pm5$ W/(m^{2}K).

Fig. 7 presents the experimental and theoretical PV diagram for one phase at $T_h^{exp} = 205.6$ °C, $T_c^{exp} = 22.1$ °C.

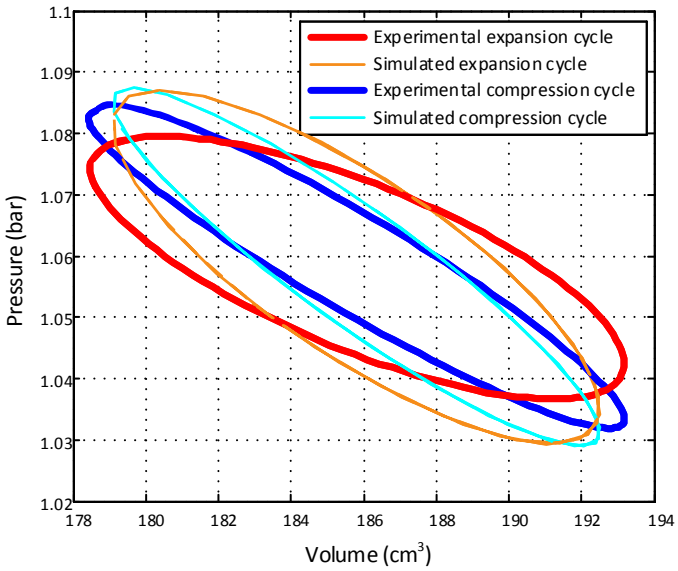

Fig. 7. Experimental and theoretical P-V diagrams

Table 1 shows the full results on the outputs values. The correlation between the model and the experiment has a maximum relative error of 8.9 %. The agreement is good, so the identified parameters will be used to validate the model on a series of experimental tests with different thermal and pressure conditions.

Table 1. Experimental and simulation results comparison

		Experimental value	Theoretical value	Difference (%)
$\dot{Q}_e$	(mW)	1253	1279	2.1
$\dot{Q}_k$	(mW)	-777	-843	8.5
amp	(mm)	3.42	3.12	-8.9
f	(Hz)	37.1	35.2	-5.1
T_e	(°C)	1701	185.9	3.4
T_k	(°C)	24.0	24.0	0.0

The hot source temperature T_h and the mean pressure p_m are modified to evaluate the accuracy of the model and the identified parameters. The comparison quantities are shown on Table 2.

It is worthy of note that the maximal difference is only 17.1 % for the amplitude and 5.1 % for the frequency of the engine. The difference between experimental and theoretical conditions is acceptable with a maximal value of 26.2 % on the compression chamber output power. Despite this error and because of the simplifications underlying the model, it is considered accurate enough.

Table 2. Correlation results

T_h (°C)		210.2		208.4		206.3		205.6	
Pressure (bar)		**1.080**		**1.070**		**1.054**		**1.015**	
amp (mm)	th	3.78	-14.9 %	3.46	-10.6 %	3.08	-17.1 %	3.12	-8.9 %
	exp	4.44		3.87		3.72		3.42	
f (Hz)	th	35.50	-3.7 %	35.37	-4.3 %	35.2	-4.6 %	35.23	-5.1 %
	exp	36.9		36.97		36.88		37.12	
$\dot{Q}_e$ (mW)	th	1 926	-8.6 %	1 597	-1.0 %	1 247	-22.2 %	1 279	2.1 %
	exp	2107		1 612		1 602		1235	
$\dot{Q}_k$ (mW)	th	-1 273	0.0 %	-1 054	-26.2 %	-822	6.7 %	-843	8.5 %
	exp	-1 273		-835		-880		-777	

4. Optimization

The electrical conversion is taken into account in this section. The equivalent electrical network studied is presented on Fig. 8, where the electromechanical transducer model presented in section 2.2 is included in the EENM. This section presents the results of the sensitivity analysis of the engine to the electrical load resistance R_c for optimization.

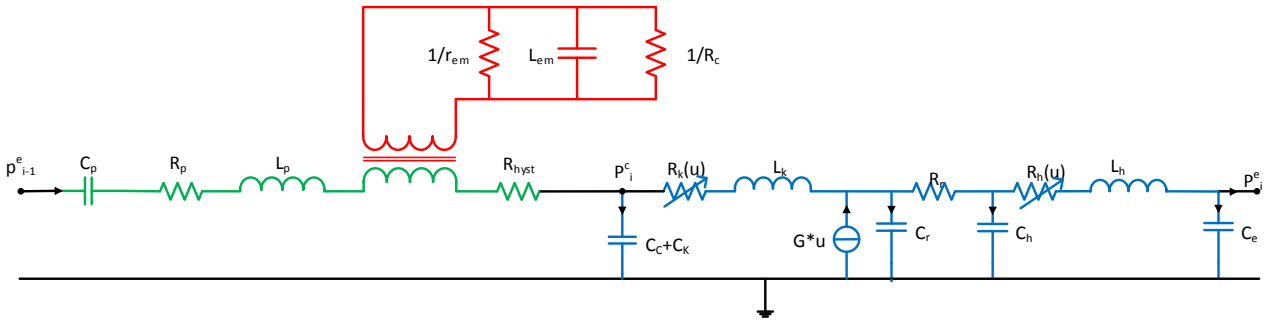

Fig. 8. Equivalent Electrical Network Model with energy conversion

The thermal-EENM approach has been used to study the influence of three main parameters and define their optimal values considering technical constraints in our engine: dead volume of the chambers, resonance frequency of the mechanical parts and insulation between the two sides. The chosen optimal parameters are: a mass of 1.64 kg, a dead volume of 50 cm^3, and a conduction resistance of 8.96 K/W.

The electromagnetic transducer geometry and coupling coefficient are taken from [13]. Its nominal diameter is 170 mm, with a voice coil diameter of 38 mm. It weighs 2.2 kg, but the oscillating mass is 17 g. The coupling coefficient is β = 9.6 N/A, and the internal resistance is r_{em} = 5.4 Ω.

The optimization here can be read as an impedance adaptation. Indeed, studying the influence of the load resistance, it is possible to obtain the maximum of either the useful power or the efficiency. Therefore, it is possible to choose the best value for the operating of the system.

The maximum efficiency is reached with a load resistance of 5.97 Ω, as shown on Fig. 9c. On this simulated operation, the power reaches 6.26 W whereas the peak-peak amplitude of the oscillations is 21.7 mm. The maximum power of 6.72 W is obtained with a resistance value of 9.55 Ω.

The load resistance has no influence on the operating frequency, which remains stable at 25.18 Hz.

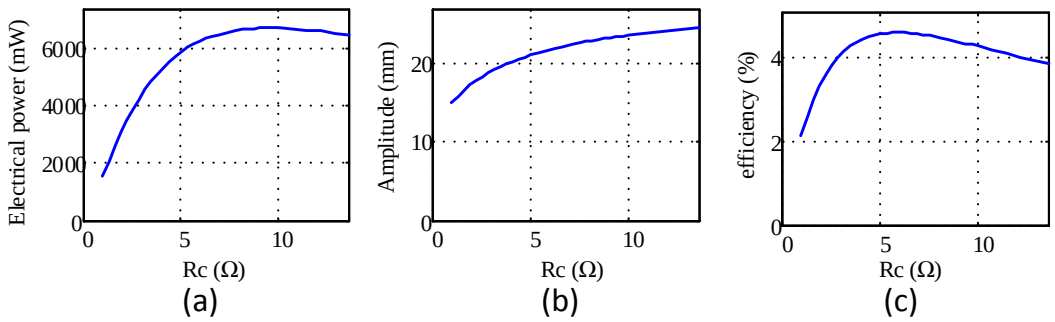

Fig. 9. Influence of the load resistance on power (a), amplitude (b) and efficiency (c)

A balance of maximum efficiency and power is obtained using an intermediate value of the resistance. Fig. 10 shows the related output electrical currents for the three phases. The output power is 6.63 W and the global efficiency is 4.51 %. The internal temperatures are T_e = 174.0 °C and T_k = 41.2 °C. The simulated internal efficiency is $\eta = \frac{P_{elec}}{\dot{Q}_e} = 5.4$ %, which represents 18.3 % of the Carnot efficiency.

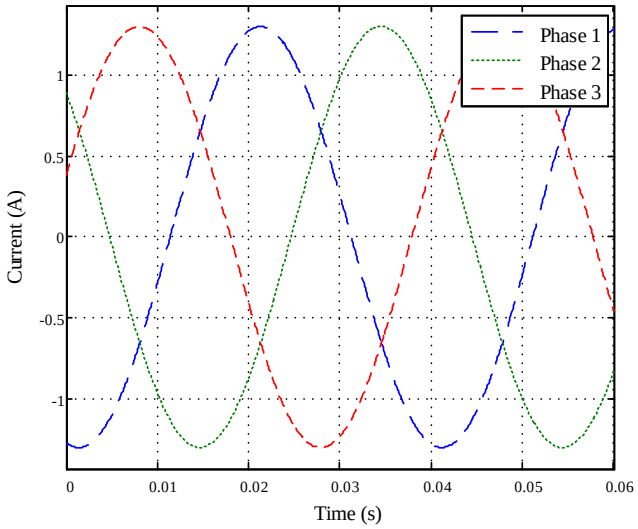

Fig. 10. Output current

5. Conclusion

A new modeling approach suitable for free piston Stirling engine has been proposed. It takes into account the non-linear pressure losses, gas inertia and the heat exchange with the external sources. The electromagnetic electromechanical conversion is also integrated. The model has been compared to experimental data from a fully instrumented prototype and the correlation is good enough for performance prediction.

A maximum electrical power of about 20 W is expected to be obtained from a 200 °C heat source. This preliminary result is promising since further components optimization will be performed. The heat exchanger and regenerator especially will have to be dealt with. The model will also be further improved. The correlation between heat exchanger coefficients, their geometry and the operation conditions (gas flow rate) will be taken into account especially.

Acknowledgement

Funding for this project was provided by a grant from la Région Rhône-Alpes and by the French National Research Agency (ANR) under grant no. ANR-12-SEED-0005-01 (MISTIC Project).

Nomenclature

A area, m^2

amp stroke, m

C equivalent capacitance, m^3/Pa

c_p specific heat, J/g.°C

D Damping, N/(m/s)

d hydraulic diameter, m

f frequency, Hz

h global convective exchange coefficient, $W.m^{-2}K^{-1}$

i current , A

k spring stiffness, N/m

L equivalent inductance, kg/m^4

m mass, kg

p pressure, bar

P mechanical power, W

$\dot{Q}$ heat power, W

r electrical resistance, Ω

R equivalent resistance, $Pa.s.m^{-3}$

t time, s

T temperature, °C

u,v gas flow rate, m^3/s

V volume, m^3

Greek symbols

β *coupling coefficient, N/A*

δ thermal penetration depth, m

η efficiency

μ dynamic viscosity, kg/(m.s)

ρ volumetric mass, kg/m^3

ω pulsation, s^{-1}

Subscripts and superscripts

c cold

e expansion

elec electrical

g gas

h hot

hyst hysteresis

k compression

m mean

p piston

t transducer

References

[1] Bianchi M, De Pascale A. Bottoming cycles for electric energy generation: Parametric investigation of available and innovative solutions for the exploitation of low and medium temperature heat sources. Appl Energy 2011;88:1500–9.

[2] Thombare DG, Verma SK. Technological development in the Stirling cycle engines. Renew Sustain Energy Rev 2008;12:1–38.

[3] Kongtragool B, Wongwises S. A four power-piston low-temperature differential Stirling engine using simulated solar energy as a heat source. Sol Energy 2008;82:493–500.

[4] Finkelstein T, Organ AJ. Air Engines. 2001.

[5] Der Minassians A, Sanders SR. Multiphase Stirling Engines. J Sol Energy Eng 2009;131:021013.

[6] Der Minassians A. Stirling engines for low-temperature solar-thermal-electric power generation. 2007.

[7] Urieli I, Berchowitz D. Stirling cycle engine analysis. 1984.

[8] Formosa F, Badel A, Lottin J. Equivalent electrical network model approach applied to a double acting low temperature differential Stirling engine. Energy Convers Manag 2014;78:753–64.

[9] Solanki R, Mathie R, Galindo A, Markides CN. Modelling of a two-phase thermofluidic oscillator for low-grade heat utilisation: Accounting for irreversible thermal losses. Appl Energy 2013;106:337–54.

[10] Swift GW, Garrett SL. Thermoacoustics: A Unifying Perspective for Some Engines and Refrigerators. J Acoust Soc Am 2003;113:2379.

[11] Nam K, Jeong S. Novel flow analysis of regenerator under oscillating flow with pulsating pressure. Cryogenics (Guildf) 2005;45:368–79.

[12] Arroyo E, Badel A, Formosa F, Wu Y, Qiu J. Comparison of electromagnetic and piezoelectric vibration energy harvesters: Model and experiments. Sensors Actuators A Phys 2012;183:148–56.

[13] Yu Z, Saechan P, Jaworski AJ. A method of characterising performance of audio loudspeakers for linear alternator applications in low-cost thermoacoustic electricity generators. Appl Acoust 2011;72:260–7.